

CFD STUDY FOR ASSESSMENT OF AXIAL THRUST BALANCE IN CENTRIFUGAL MULTISTAGE PUMPS

Stefania DELLA GATTA¹, Simone SALVADORI², Paolo ADAMI³,
Laura BERTOLAZZI⁴

¹ Corresponding Author. Department of Energetics, University of Florence. Via S.Marta, 3 50139 Florence, Italy. Tel.: +39 055 4796239, Fax: +39 055 4796342, E-mail: stefania.dellagatta@unifi.it

² Department of Energetics, University of Florence. E-mail: simone.salvadori@unifi.it

³ Department of Energetics, University of Florence. E-mail: paolo.adami@unifi.it

⁴ Weir Gabbioneta Srl. V.le Casiraghi. 68 20099 Sesto S. Giovanni (MI), Italy. E-mail: laura.bertolazzi@weirgabbioneta.com

ABSTRACT

Present work aims to the numerical investigation of horizontal multistage centrifugal pumps in opposite impeller configuration. Its main target is to apply a three-dimensional CFD based tool to the axial thrust prediction in a multistage industrial machine. A flexible use of CFD is presented to extend the hydraulic behaviour evaluation for the single components to the whole pump characterization. A mixing plane technique has been chosen to study the interaction between rotating and stationary parts. This procedure takes into account the effects of different incidences and inlet velocity distortions.

The 3D CFD investigation on every single component of the multistage pump allows a thorough knowledge of its fluid dynamic fields, but only a correct matching and interpretation of all the components provide a reliable prediction of pump axial thrust as well as its performance curve. Despite the potential high degree of realism allowed by CFD, modelling the whole pump geometry may be quite expensive. In fact, the pump includes a great amount of components and several geometrical details (i.e. inlet and outlet volutes, inter-stage cross-over, leakages through wear rings and balancing drums) that have to be taken into account for a good prediction of the axial thrust. These issues lead to a consistent amount of numerical modelling problems which are considered and discussed.

Keywords: Axial Thrust, CFD, Multistage centrifugal pumps.

NOMENCLATURE

A	$[m^2]$	passage area
BEP	$[-]$	Best Efficiency Point
d	$[m]$	diameter

g	$[m/s^2]$	gravity
H	$[m]$	head
k, a, b, c	$[-]$	coefficients
L	$[m]$	passage length
\vec{n}	$[-]$	normal vector
p	$[Pa]$	pressure
Q	$[m^3/s]$	flow rate
r	$[m]$	radial local coordinate
R	$[m]$	impeller radius
Re	$[-]$	Reynolds number
T	$[N]$	thrust
u	$[m/s]$	blade velocity
v	$[m/s]$	velocity
ω	$[s^{-1}]$	local fluid rotational speed in front and back impeller chambers
Ω	$[s^{-1}]$	rotating speed

Subscripts and Superscripts

ax	axial
θ	tangential

1. INTRODUCTION

Residual axial thrust in centrifugal pumps is usually balanced by axial thrust bearings, whose correct and proper design is highly important for the mechanical reliability of the pump itself.

Moreover, a deep knowledge of the components contributing to the axial thrust is of relevant interest. The flow field contribution to the hydraulic axial thrust is mainly realized in the impeller but is also affected by the presence of leakages flows inside the gaps between impeller and casing walls.

Thereby, a numerical investigation of the phenomenon should not be limited to the analysis of the impeller flow field but it has to be extended to the whole machine detailed in its single components.

Present paper is concerned with the investigation of a multistage centrifugal pump designed and produced by Weir Gabbioneta whose section is reported in Figure 1 and whose very complex layout will be described in detail in the next paragraph. As it is evident, the achievement of such a complex task requires the development of a strategy dealing with all the following items:

- The analysis of the single stages, including both rotating and stationary components;
- The study of the flow conditions inside the front and back shroud impeller side chambers and balancing drums and the evaluation of their contribution to the axial thrust;
- The final data collection and processing in order to assess and verify the residual hydraulic axial thrust.

The strategy developed for each single issue will be described in detail and the results of its application to the centrifugal pump in Figure 1 will be presented and discussed here below.

2. MULTISTAGE PUMP GEOMETRY

Present work investigates a five stages horizontal centrifugal pump (Figure 1).

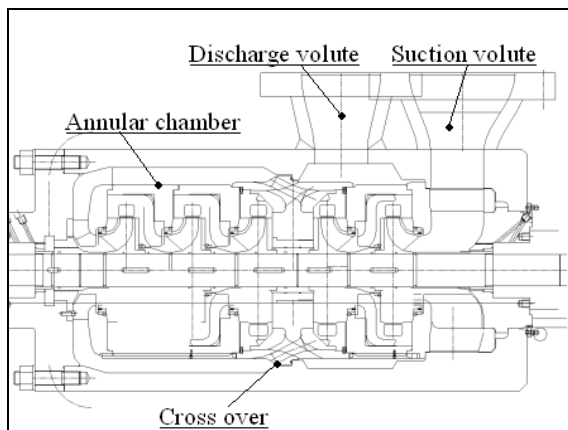


Figure 1. Layout of the investigated multistage centrifugal pump in opposite impellers configuration

Axial thrust balance is primarily obtained thanks to the opposite impeller configuration characterized by the opposite flow direction in the first two stages and in the last three ones. A crossover device leads the flow from the first to the second group of stages through an annular chamber, thus being responsible for the turning of the flow direction. Axial unbalance is evident for the investigated pump due to a different impellers number in the opposite groups of stages, but also in pumps with even impeller number the axial balance is not to be taken for granted due to the presence of leakages flows.

Thrust bearings are then required. To design them correctly, the presence of the impeller side

chambers (Figure 2) and balancing drums has to be considered.

The leakage flow in the side chambers can help to reduce the axial thrust, but only penalizing pump efficiency.

In such a complex machine, three kinds of cavities are present: front and back impeller shroud cavities and a central drum. Two of them (the front and the back shroud chambers) are reported in Figure 2.

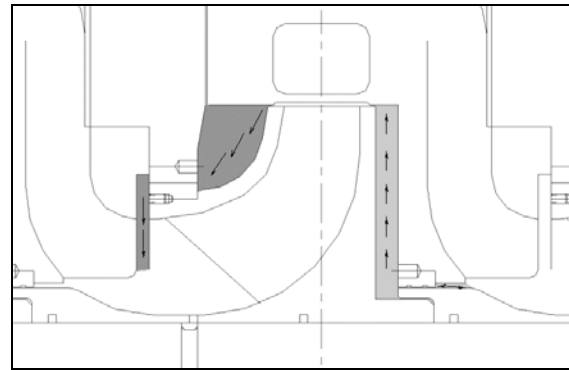


Figure 2. Front and back impeller side chambers for an intermediate stage

While the flow inside the front shroud chamber always radially turns inward, the one inside the back shroud cavity can also radially turn outward depending on different positions. Even if, in this case, mass flow passing through the back shroud chamber has a slight influence on the whole pump performance, its contribution to the axial thrust can not be neglected.

The central balancing drum (Figure 3) is located between the second and the fifth impellers, next to the crossover device. Flow direction is shown in Figure 3.

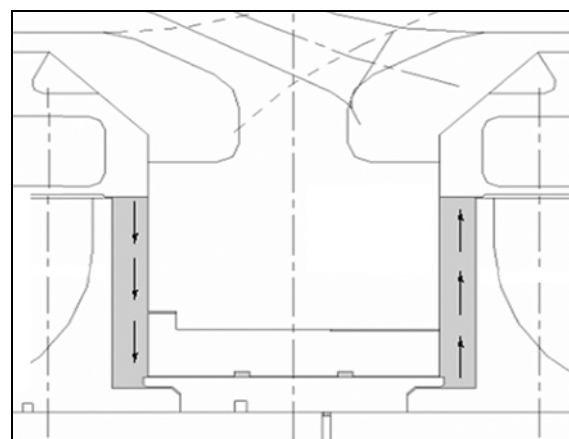


Figure 3. Central balancing drum between the second and the fifth stage

The lateral balancing drum (reported in Figure 4) is located between the first impeller of the second group of stages. A balancing duct connects the drum to the suction nozzle, thus keeping the value

of suction pressure at the external side of the drum itself.

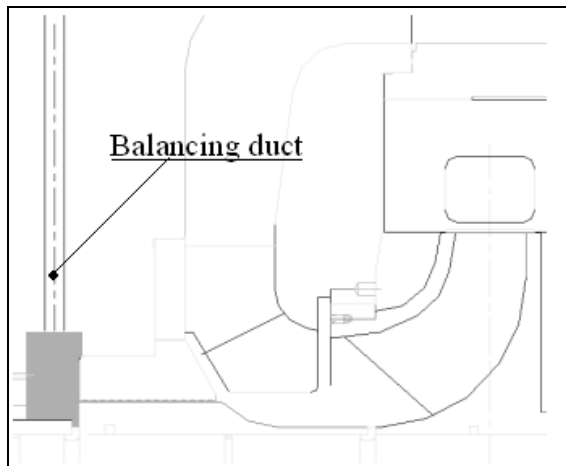


Figure 4. Lateral balancing drum between the first and the second group of stages

All diffusers are characterized by the same vanes except for the second and the fifth which face the crossover. All the impellers are geometrically identical, but have different inlet conditions due to the presence of different static upstream components (i.e. the first impeller follows the suction volute while the third one follows the cross over device annular chamber).

3. NUMERICAL INVESTIGATION FEATURES

Several 3D steady simulations solving RANS (Reynolds Averaged Navier Stokes) equations have been carried out in the fluid domain. Standard techniques have been employed for the numerical computation: a finite-volume pressure-correction procedure for incompressible flow has been employed and a two-equation $k-\varepsilon$ turbulence model with standard wall functions has been applied.

Pump main components have been analysed separately in order to reduce computational costs. Even the side chambers flow has been analysed with 2D CFD simulations apart from the main flow inside impeller and diffuser. Furthermore, as stated by Gantar et al. [1] for a geometry which was very similar to the present one, an eventual flow recirculation in impeller exit/diffuser inlet area does not impact on the impeller side chambers. This probably happens because the main impeller passages and the side chambers are sufficiently separated by throttling via a small clearance.

Summarizing, because of their different geometry, the following elements have been modelled:

- Suction volute;
- First impeller;

- Each diffuser not facing the crossover device coupled with its downstream stage impeller,
- Second diffuser and crossover device;
- Third impeller;
- Fifth diffuser and discharge volute;
- Impeller front shroud side chamber;
- Impeller back shroud side chamber;
- Central balancing drum;
- Lateral balancing drum and balancing duct.

Finally, all the results have to be combined in order to obtain the axial thrust of each of the two groups of stages, thus helping to understand their reciprocal balancing effects.

3.1. Stage coupling approach

The hydraulic axial thrust on the machine shaft is due to the pressure integral on the impeller walls. However, simulations of the stationary components are still required to calculate the performance of the whole pump and to provide the correct boundary conditions for the rotating components calculation.

The presence of both rotating (impeller) and stationary (diffuser) parts inside each stage requires a strategy to couple them, namely to deal with the computation of two domains characterised by a different periodic condition because of the different number of blades.

A mixing plane approach has been selected for present study. It allows to solve separately the rotating and the stationary domains in steady conditions. The flow field data from adjacent zones have been imposed as spatially averaged boundary conditions or “mixed” at the mixing plane interface.

This approach removes any unsteadiness deriving from the circumferential variations in the passage-to-passage flow field, thus yielding a steady-state result. However, despite the simplifications, several applications demonstrate that the approximation of the time-averaged results is quite reasonable.

As further hypothesis, the stage kinematic repeatability has been assumed. Therefore, the velocity profile at the impeller exit has been employed to update the diffuser inlet boundary condition.

The whole process can be synthesised in these main steps:

- Solution of the Navier-Stokes equations in both domains;
- Average of the flow in tangential direction;
- Update of the boundary conditions;
- Iteration of the previous steps until convergence is achieved for profiles of velocity and pressure.

The spatial discretisation consists approximately of 500.000 elements both for impeller and diffuser. The surfaces selected for mixing plane and for stage repeatability are reported in Figure 5.

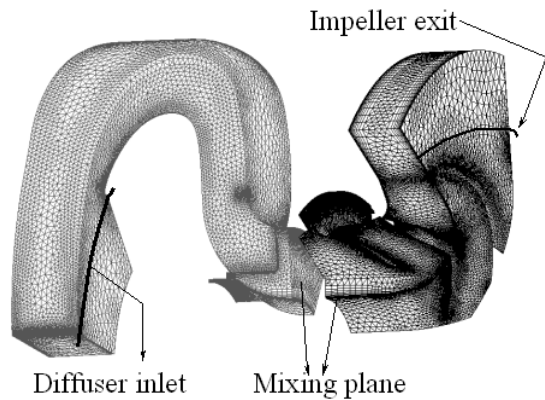


Figure 5. Geometrical domains and surfaces for the stage coupling

Impeller-diffuser interactions is not limited to the main flow, but also involves the leakage flow that considerably affects both the axial thrust and the efficiency of the whole pump.

Leakage flow analysis will be discussed in detail in the next paragraph. To consider the leakage flow entering and exiting from impeller and diffuser, the outward part of the side chamber has been modelled in their geometric domain. For example, the impeller geometric domain has been modelled including the boundary corresponding to the stage interface with the internal leakage flow.

A constant leakage distribution across axial and circumferential extents of the interfaces between main flow and cavities has been assumed. Furthermore, it has been verified that the geometries are not sensitive to the direction of the injection velocity, thus confirming leakage mass flow as the most significant parameter.

For this reason, to impose boundary conditions at these interfaces the leakage mass flow dependency on impeller head has to be considered. Then, the boundary conditions need to be uploaded during the computation by checking the actual value of impeller head. This constitutes a further step coupled to the ones previously listed. The procedure is reported in Figure 6.

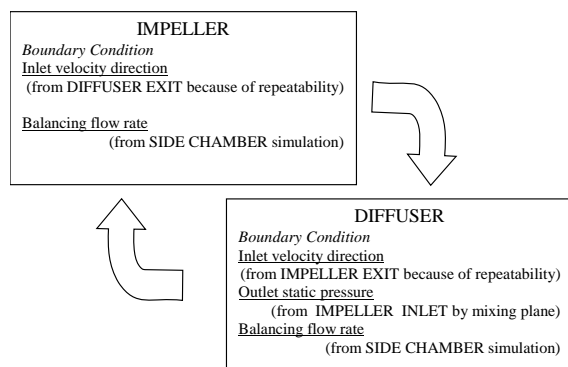


Figure 6. Scheme of the complete coupling procedure

All the CFD analysis have been repeated for different capacities.

Finally, the characteristic curve for the whole pump has been obtained. Its dimensionless version is shown in Figure 7.

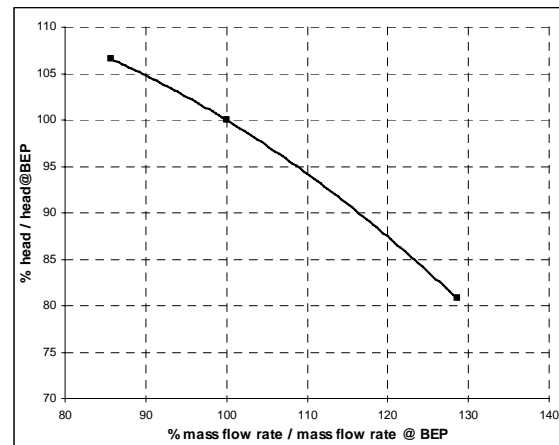


Figure 7. Pump dimensionless characteristic curve

3.2. Impeller side chambers

Impeller side chambers have been studied by means of a 2D-CFD approach. The hypothesis of axial symmetry has been reasonably assumed for this problem.

The flow inside the cavity is radially outward at the rotating wall, while it is radially inwards at the casing wall. The internal flow of the impeller side chamber presents a core zone between the casing-diffuser stationary wall and the impeller rotating one. The central core rotating speed is lower than the impeller one (Batchelor, [2] and Stewartson, [3]).

The rotating velocity inside the chambers depends on peripheral conditions, namely on the impeller rotating speed and on the head across the cavity itself. Due to pump geometry, head across the leakage corresponds to impeller head. Therefore, leakage mass flow and its contribution to the axial thrust depend on pump working conditions.

Results from the front shroud chamber analysis are discussed as exemplification here below and details of the corresponding computational grid (approximately 50.000 elements) are shown in Figure 8.

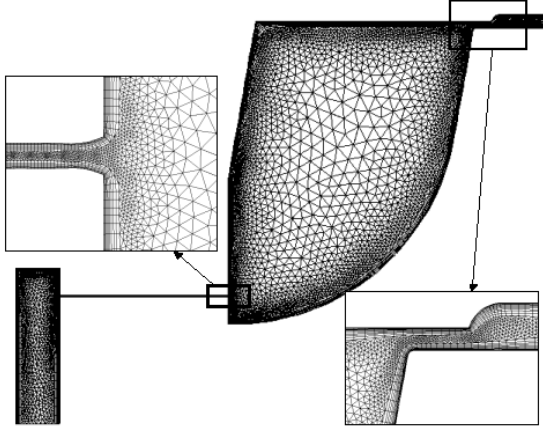


Figure 8. Details of the computational grid of the front shroud impeller chamber

To get an exhaustive leakage characterization, the CFD analysis has been performed for different heads across the cavity and calculating the corresponding leakage mass flow.

These results can be employed to tune some well known correlations from the literature (Traupel [4], Utz [5], Denny [6], Wortster et al. [7]) which allow to update stage analysis boundary conditions in a simple and quick way reaching a good accuracy. By such a way, cavity flow is solved at different operating points in a preliminary phase, but does not require to be calculated at every update of the stage coupling boundary conditions.

As far as leakage mass flow rate is concerned, the correlations take into account wear rings geometrical characteristics, rotational speed and impeller head as follows:

$$Q_p = k\sqrt{2gHC_d} A \quad (1)$$

$$C_d = \left(\frac{1}{\lambda \frac{L}{d}} + a \right)^{0.5} \quad (2)$$

$$\lambda = \frac{b}{\text{Re}^{0.25}} \left[1 + 0.5 \left(\frac{u}{v} \right)^2 \right]^c \quad (3)$$

Here Q_p is the leakage flow rate, H the head, A the passage area, L the passage length, d the seal diametral clearance, u the blade velocity, v the mean flow speed inside the seal. Coefficients (a , b , c) depend on geometrical characteristics.

The leakage mass flow is obtained as a function of the head across the cavity (Figure 9).

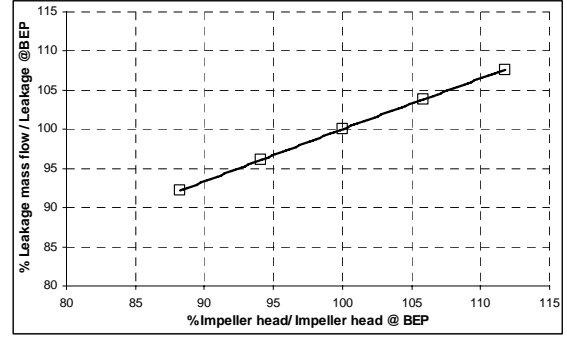


Figure 9. Non-dimensional leakage mass flow rate against non-dimensional impeller head (front shroud impeller chamber)

Head across the cavity results in a centripetal flow with radially inwards structures at the stationary wall and outwards ones at the rotating walls. Local tangential velocity divided by the impeller velocity:

$$\frac{v_g}{u} = \frac{v_g}{\Omega r} \quad (4)$$

has been reported in Figure 10 together with the streamlines inside the cavity.

In the same way, the dimensionless rotating velocity inside the cavity can be defined as follows:

$$\frac{\omega}{\Omega} = \frac{v_g}{r} \quad (5)$$

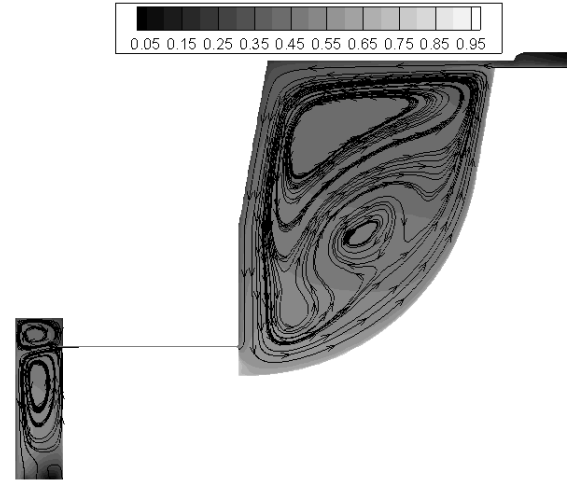


Figure 10. Non-dimensional tangential velocity distribution inside the front shroud impeller chamber

Figure 11 shows the back shroud impeller chamber grid and the corresponding tangential velocity distribution.

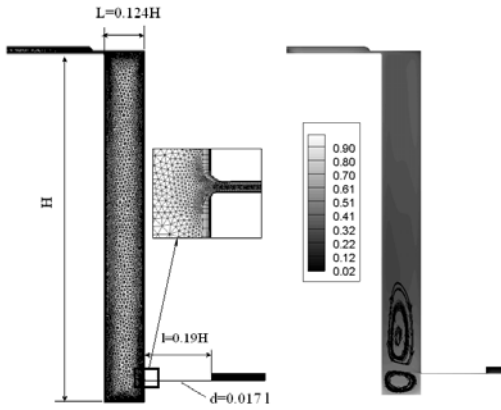


Figure 11. Details of the computational grid and non-dimensional tangential velocity distribution inside the back shroud impeller chamber

Repeating calculations showed that peripheral velocity with respect to the impeller one depends on the mass flow condition through the cavity. The dimensionless rotating velocity distribution in the middle of the cavity is reported in Figure 12 at different flow rates.

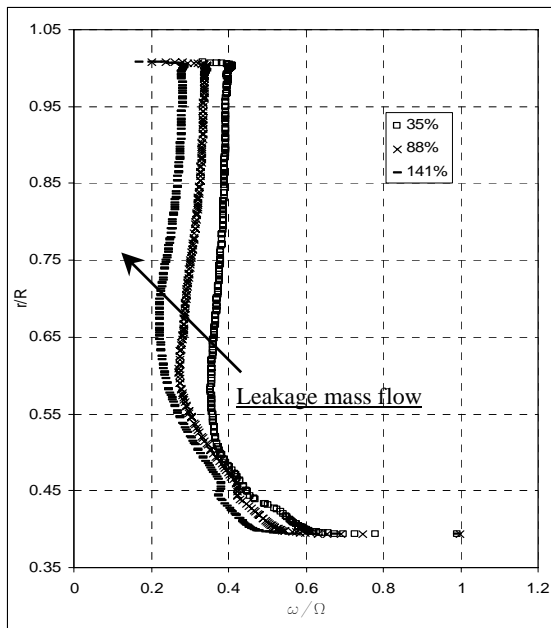


Figure 12. Dimensionless rotating velocity inside the back impeller cavity at different mass flow rates (referred to the leakage mass flow at BEP)

Fluid rotating speed inside the cavity presents a typical value for dimensionless radius ranging from 0.55 to 1. The typical characteristics of the Batchelor flow (Batchelor, [2]) can be observed, namely, the fluid rotates as a solid body between two boundary layers. For the internal regions, the distribution called as Stewartson flow (Stewartson, [3]) is encountered, with the classic “vortex” distribution.

Increasing the mass flow through the cavity, the presence of the Stewartson distribution is increased,

while the value of constant rotating velocity of the core flow is reduced.

This agrees with the results of Debuchy et al. [8]. The conclusion was that the Batchelor type flow can be observed at low mass flow rates, and far from the periphery because of the influence of the inlet conditions. It was also found that the flow structure near the axis is strongly affected by a weak stream, which enhances the level of the core-swirl ratio near the axis.

Pressure distribution on the back and front shroud of the impeller is qualitatively reported in Figure 16, while in Figure 17 the pressure distribution is reported for the second and the fifth impeller back shroud.

The pressure distribution inside the central drum is highly influenced by the flow conditions. The most important parameters are the leakage mass flow rate and the head across the cavity which depend on pump operating conditions, on the main flow rate and on wear rings clearance. Present work has been carried out with fix design values for these clearances. However, during its life, the real pump will undergo a process of wear resulting in wear rings clearance enlargement and consequent increase of leakage flow, global performance worsening and residual axial thrust modifications as far as module and sometimes direction is concerned.

In Figure 13, the radial distribution of static pressure inside the back shroud cavity is reported. A different value of leakage flow rate divided by the leakage flow rate at BEP corresponds to each curve. All the curves are plotted considering the same reference pressure at the impeller exit.

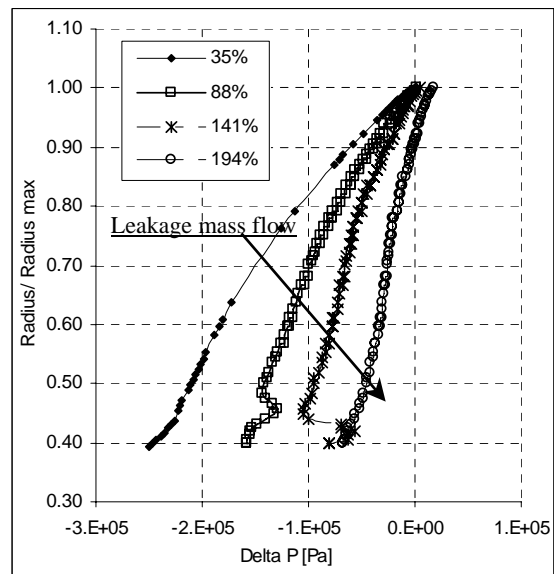


Figure 13. Radial distribution of static pressure inside the back shroud chamber at different mass flow rates

Let consider now the same distribution divided by a term expressing the centrifugal force:

$$\Delta p' = -\frac{\Delta p}{\rho \omega^2 r^2} \quad (6)$$

as reported for different mass flow in Figure 14.

It should be remember that ω expresses the local fluid rotational speed in front and back impeller chambers and r the local radial coordinate.

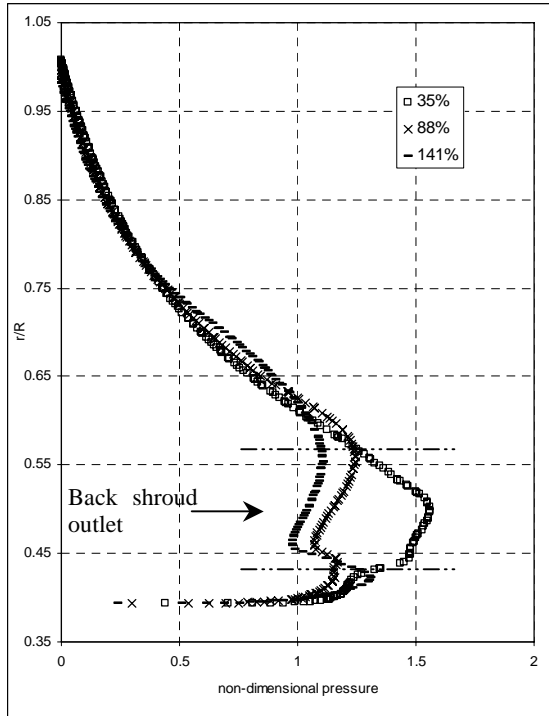


Figure 14. Radial distribution of dimensionless pressure inside the back shroud chamber at different mass flow rates

It should be observed that all curves are coincident except between $r/R=0.45$ and $r/R=0.55$, where the outlet of the back shroud chamber is located.

The integral of the pressure distribution is here down plotted as axial thrust against leakage mass flow (Figure 15).

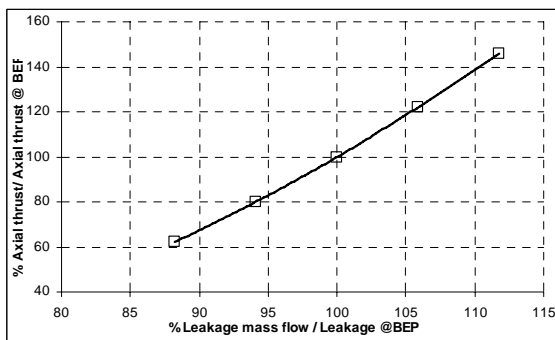


Figure 15. Non-dimensional axial thrust vs. non-dimensional impeller head (back shroud chamber)

The rate of this dependency is quite high. Considering for example a variation of 12% in the back shroud leakage mass flow, a 50% increase in axial thrust is observed. For this reason, the choice of a cavity geometry oriented to reduce leakage mass flow is of relevant importance in balancing the axial thrust.

3.3. Axial thrust calculation

To calculate the axial thrust acting on the whole machine, both the contribution of the main and of the leakage flows have to be considered.

With reference to the single stage, the hydraulic axial thrust acting on the impeller is given by the contribution of the inlet flow and of the front and back shroud leakages flows (Figure 16). The back shroud helps to balance the machine by contrasting the thrust due to impeller and front shroud.

The hydraulic thrust is gathered from the wall pressure distribution obtained by CFD calculations:

$$T_{ax} = \int_A p \bar{n} dA \quad (7)$$

As regards the cavities, the axial thrust is calculated adding a constant pressure outlet value and of a term due to the pressure distribution on the rotating wall. Then,

$$\begin{aligned} T_{ax,cavity} &= \int_A p_{exit,impeller} \bar{n} dA + \int_A p \bar{n} dA = \\ &= p_{exit,impeller} \int_A \bar{n} dA + \int_A p \bar{n} dA \end{aligned} \quad (8)$$

where the area is referred to both the front and back impeller shroud chambers.

Similarly the axial thrust is calculated for central and lateral balancing drums.

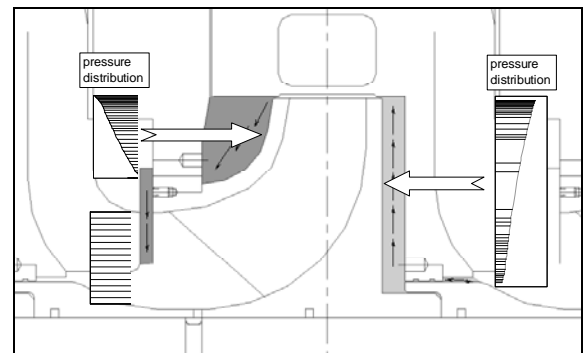


Figure 16. Leakage contributions to the axial thrust

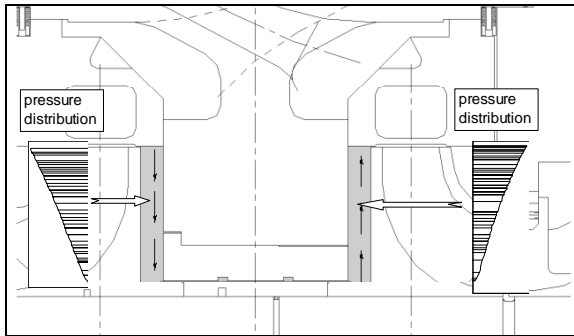


Figure 17. Central balancing drum contributions to the axial thrust

Considering the actual alignment of the stages (shown in Figure 1), these results are extended to the whole machine.

Each component contribution to the axial thrust is reported in Figure 18 and Figure 19.

It can be easily verified that the greater contribution is due to the central balancing drum where the flow is driven by pump head and by wear rings clearances eventually modified by mechanical wear. The sum of all these contributions gives a global thrust estimation.

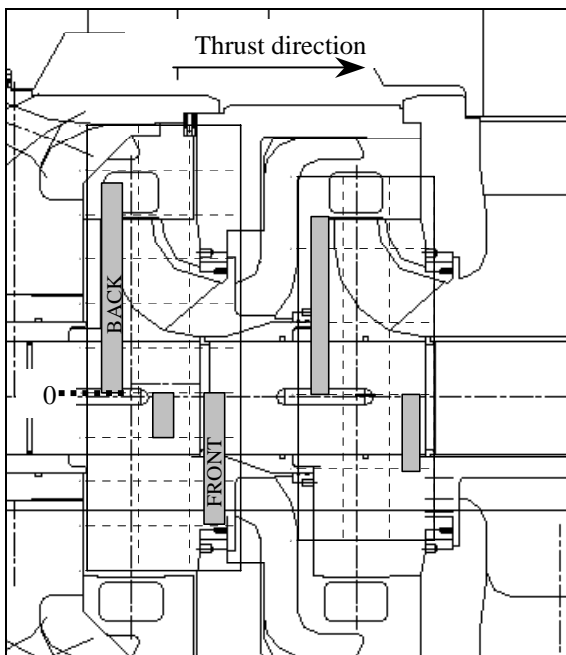


Figure 18 . Effects of the first group of stage on the global axial thrust. The arrow direction refers to the global axial thrust direction.

Although the opposite alignment of the two groups of stages, the global thrust is not null and it is directed as shown by the arrows in Figure 18 and Figure 19.

For a proper design of the thrust bearings, it is still required to know the maximum thrust in pump operating range. Data from manufacturers indicate machine operating conditions between the 80% to the 120% of the BEP flow rate as the preferred

operating region. The axial thrust trend in this operating range is reported in Figure 20.

The maximum thrust for the investigated pump is obtained at the lower mass flow, where the total head of the pump is maximum. Really, the machine operating range goes down to the minimum continuous flow. Other analysis have to be carried out to investigate pump behaviour for different range and to verify the increase of residual axial thrust for lower capacity.

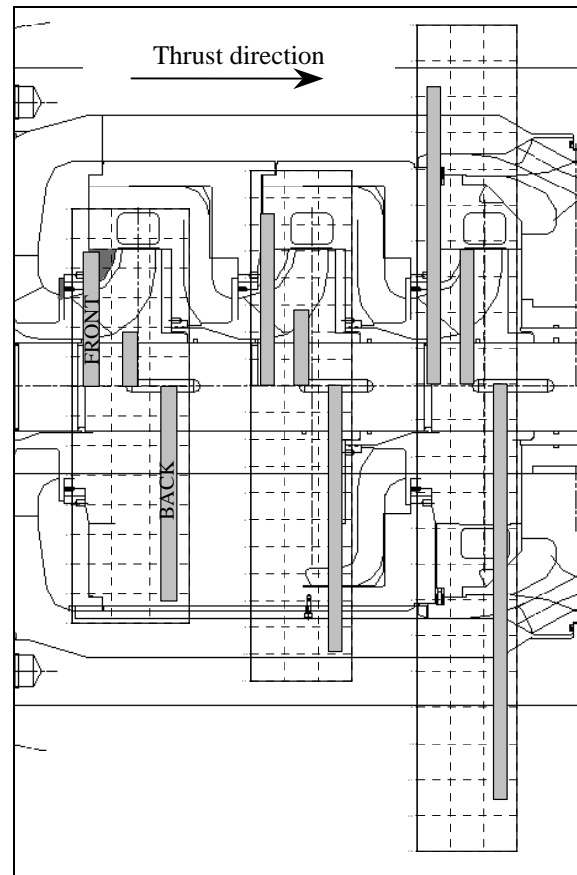


Figure 19. Effects of the second group of stage on the global axial thrust. The arrow direction refers to the global axial thrust direction.

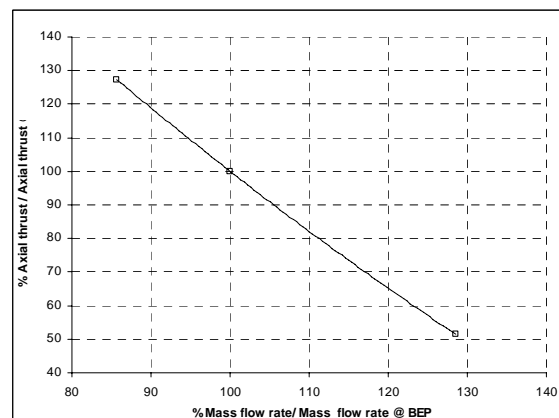


Figure 20. Global dimensionless axial thrust against main flow rate

4. CONCLUSIONS

A numerical investigation of a multistage centrifugal pump has been carried out. Driving the correct design and dimensioning of the axial bearings to balance the hydraulic thrust is the present study main target.

To reach the task, both the main, the impeller chambers and the balancing drums flow have to be considered because of their relevance to the problem of axial load unbalance.

Separated CFD analysis have been carried out for stage (with a mixing plane approach) and side chambers. 2D analysis to characterize the central drum and the lateral balancing drum have been developed.

A methodology to predict the residual axial thrust for a complex machine has been presented and pump sensitivity to the different variables which influence axial thrust have been pointed out.

Actual results show the calculated characteristics maps of the pump and how the axial thrust depends on the operating conditions of the pump as well as its mechanical wear conditions, because of effects on the main flow head and on the pressure distribution inside the side chambers.

Furthermore, it has been highlighted that side chambers give a great contribution to the axial thrust and that their pressure distribution is highly influenced by leakage mass flow and by local rotating speed inside the cavity.

ACKNOWLEDGEMENTS

The authors are grateful to Prof. Ing. F. Martelli of University of Florence, Ing. G. Marengo, Ing. D. Maestri and Ing. A. Piva of Weir Gabbioneta Srl for their valuable suggestions during the development of this work.

REFERENCES

- [1] Gantar, M., Florjancic, D., and Sirok, B., 2002, "Hydraulic Axial Thrust in multistage Pumps-Origins and Solutions", *ASME J Fluids Engineering*, Vol. 124, pp. 336-341.
- [2] Batchelor, G.K., 1951, "Note on a class of solutions of the Navier-Stokes equations representing steady rotationally-symmetric flow", *quart.J.Mech.Appl.Math.*, Vol.4, pp. 29-41.
- [3] Stewartson, K., 1953, "On the flow between two rotating coaxial discs", *Proc.Camb.Phil.Soc.*, Vol. 49, pp. 333-341.
- [4] Traupel, W., 1958, *Thermische Turbomaschinen*, Springer-Verlag, Berlin.
- [5] Utz, C., 1972, „Experimentelle Untersuchung der Strömungsverluste in einer mehrstufigen Axialturbine“, *Mitt.Ins.Therm.Turbomasch.* ETH Zurich, Nr.19.
- [6] Denny, D.F., 1954, "Leakage flow through centrifugal pump wear rings", *TN460, Beds: BHRA*, Cranfield.
- [7] Worster, R.C., and Thorne, E.W., 1959, "Measurement of leakage flow through the wearing rings of a centrifugal pump and its effect on overall performance", *Beds: RR 619*, Cranfield.
- [8] Debuchy, R., Dymont, A., Muhe, H., and Micheau, P., 1998, "Radial inflow between a rotating and a stationary disc", *Eur. J. Mech. B/Fluids*, Vol. 17, N°6, pp. 791-810.
- [9] Adami, P., Della Gatta, S., Martelli, F., Bertolazzi, L., Maestri, D., Marengo, G., and Piva, A., 2005, "Multistage turbo-pumps: Assessment of a mixing plane method for CFD analysis", *Proc. 60° ATI Conference*, Roma, Italy, ATI60-12-1.
- [10] Daily, J.W., and Nece, R.E., 1960, "Chamber dimension effects on induced flow and frictional resistance of enclosed rotating discs", *J. Basic.Eng*, Vol. 82, pp. 217-232.